

# The supremum principle selects simple, transferable models

Cody Petrie,\* Christian Anderson, Casie Maekawa, Travis Maekawa, and Mark K. Transtrum†

*Department of Physics and Astronomy  
Brigham Young University  
Provo, UT 84602*

(Dated: September 23, 2021)

Humans use analogical reasoning to connect understanding of one system to another. Can machines use similar abstractions to transfer their learning from training data to other regimes? The Manifold Boundary Approximation Method constructs simple, reduced models of target phenomena in a data-driven way. We consider the set of all such reduced models and use the topological relationships among them to reason about model selection for new, unobserved phenomena. Given minimal models for several target behaviors, we introduce the *supremum principle* as a criterion for selecting a new, transferable model. The supremal model, i.e., the least upper bound, is the simplest model that reduces to each of the target behaviors. By unifying the relevant mechanisms, the supremal model successfully transfers to new target domains. We illustrate on a simple epidemiological example and elaborate on Wnt signaling from developmental biology. We present a general algorithm for constructing a supremal model and note formal connections to theories of analogical reasoning in cognitive psychology.

One of the important purposes of mathematical models in scientific activity is to encode the assumptions that enable scientists to make new predictions from past data. These assumptions form a hypothesis space and are collectively referred to as *inductive bias* [1]. In this study, we use the geometric and topological relationships among candidate models to reason about inductive bias and model selection. Of particular interest are predictions for qualitatively different inputs than those on which a model was trained. A model’s ability to make such *out-of-domain* predictions is sometimes known as *transferability*, which is stronger than generalization, i.e., predicting data generated for inputs similar to those on which it was trained [2]. We propose a general principle of model selection, the *supremum principle*, that encodes a preference for simplicity with respect to target quantities of interest while enabling model transferability and whose construction uses topological relationships formally equivalent to models of human analogical reasoning.

A minimal criterion for a useful predictive model is accurate interpolation of training data, and common statistical practices such as holdout, jackknife, and cross-validation reinforce this standard. Sloppy models [3–6], a class of over-parameterized models, further formalize the relation between prediction and interpolation using information geometry [7, 8]. The predictions of sloppy models are controlled by only a few *stiff* parameter combinations and so are said to have a *low effective dimensionality* [8, 9]. Effective dimensionality is quantified in terms of widths of a model manifold, rigorous bounds for which are given by theorems from interpolation theory [8, 10]. Indeed, it has been suggested that predictive models are generalized interpolation schemes [11].

However, there is a sense that more than simple interpolation ought to be possible [12, 13]. Human cognition is driven by understanding, rather than mere pattern mimicry. When we reason about molecular bonds as if they were balls and springs, we use analogical reasoning to identify abstract relationships and transfer insights among superficially different systems. Can machines similarly analogize to make predictions of a qualitatively different nature than those on which they were trained?

To explore this question, we use information geometry to assess parameter identifiability and predictive performance for models fit to data from different regimes and reason about the hypotheses for which they encode. The fundamental object is the Fisher Information Matrix (FIM) that acts as a Riemannian metric on a manifold of models with parameters as coordinates [8, 14]. Model manifolds are often thin, and boundaries correspond to simplified models [15]. Distances measured by the FIM typically *compress* the model manifold into a few relevant directions [6] so that the manifold is thin and well-approximated by a low-dimensional, simplified model that resides on the boundary. Given training data, the Manifold Boundary Approximation Method (MBAM) explicitly finds limiting approximations to give a minimal, reduced model that encodes the information contained in the data.

Given several reduced models for target quantities of interest, we next seek a single model that unifies their simplified explanations. To select the appropriate model, we introduce the *supremum principle*: select the simplest model that is reducible to each of the target behaviors. We call this model the *supremal model* and give an algorithm below for constructing it. The supremum principle formally encapsulates a preference for simplicity akin to Occam’s razor, motivated by the assumption that abstract models that explain multiple behaviors are more likely to transfer accurately to novel behaviors than models developed for a single phenomenon.

---

\* codypetrie89@gmail.com

† mktranstrum@byu.edu

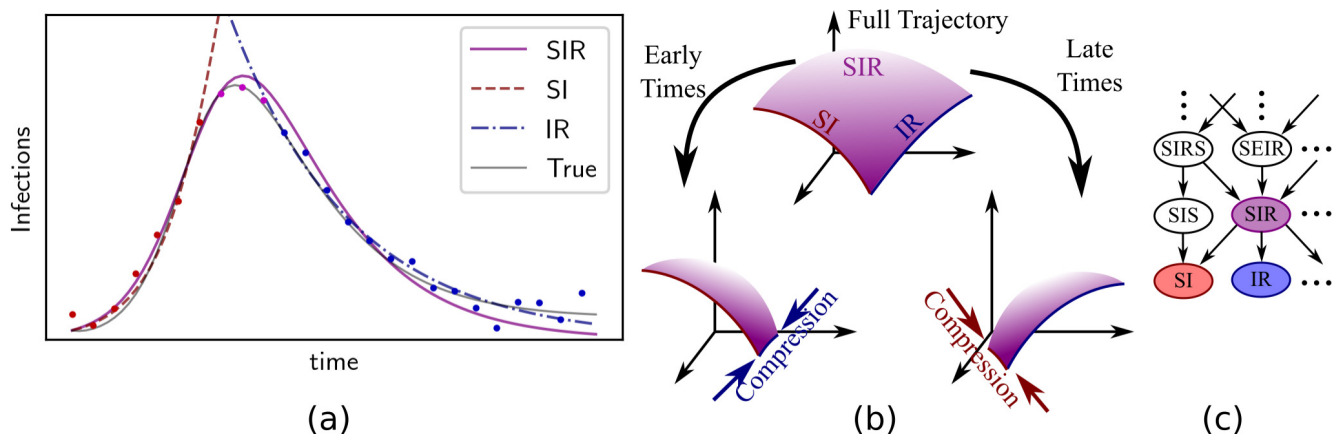


FIG. 1: (a) Infections versus time for a hypothetical epidemic. Data taken at different times—early (red), late (blue), and intermediate (purple)—exhibit qualitatively different types of behaviors. These data carry information about different aspects of the generating process. (b) Information geometry quantifies how data identify a model’s parameters. The full trajectory completely identifies an SIR model, manifest by a model manifold that is not compressed along any direction. Restricting to data at early times compresses the directions related to a recovery rate so that the model is well-approximated by an effective SI model. Similarly, restricting to late times compresses information about infection, leading to an effective IR model. (c) Candidate models of varying complexity can be arranged hierarchically in a directed graph. The SIR model is the *supremum* of the SI and IR models, i.e., the simplest model that combines information from both early and late times. It can use the information from data in two of the regimes to accurately predict a third.

As a motivating example, consider modeling infection trajectories during an epidemic. Fig. 1a shows data generated from an MSEIR model with birth and death rates (six parameters, fifth-order dynamics) and corrupted by Gaussian noise. We partition the data into three qualitatively distinct regimes—early (red), intermediate (purple), and late (blue)—and ask: Which subsets of the data are informative for predicting data in another regime?

To illustrate the key principles, consider fitting the data with a simple SIR model (two parameters, second-order dynamics),

$$\frac{dS}{dt} = -\beta I \frac{S}{N}, \quad \frac{dI}{dt} = -\gamma I + \beta I \frac{S}{N}, \quad \frac{dR}{dt} = \gamma I. \quad (1)$$

When fitting to qualitatively different data, the two-dimensional SIR model manifold is compressed depending on the informativity of the available data. The compression determines which parameters are identifiable from data and leads to an appropriate reduced model.

We focus on two reduced models on the boundary of the SIR model, shown in Fig. 1b. The first boundary segment, corresponding to  $\gamma \rightarrow 0$ , is the model with no recovery compartment, i.e., an “SI” model. Similarly, the “IR” model with  $\beta \rightarrow \infty$  has a very fast infection rate. Consider only data from early times (red in Fig. 1). The FIM compresses the model manifold along the SI boundary segment, rendering the recovery rate  $\gamma$  irrelevant. The approximate SI model (red dashed line in Fig. 1) has an effective infection rate that fits the early exponential growth [16]. However, recovery data at later stages (blue), render  $\beta$  irrelevant and are well approximated by the IR model.

The SI and IR models interpolate in their respective domains, but do not transfer beyond their training set. The SIR model is the simplest that can interpolate all three regimes. Formally, the hierarchy of potential models forms a graded Partially Ordered Set (POSet), and the directed graph (Fig. 1c) is known as a Hasse diagram [17]. In this formalism, the SIR model is the *supremum* (i.e., least upper bound) of the SI and IR models as it is the simplest model that reduces to both. The topological relationships (the adjacency relationships summarized in the Hasse diagram) among candidate models enable reasoning about the mechanisms at play in diverse contexts and inform the construction of the supremal model that combines these mechanisms in a minimal way. The resulting supremal model enables predictions of a qualitatively different type from those on which it was trained. Constructing a supremal model is not always as straightforward as in this example, but the process can be formalized as we demonstrate for the Wnt signaling pathway.

The Wnt signaling pathway is the dominant mechanism in almost all animals by which short-range extracellular signals are relayed to the nucleus to trigger local cell division during development and stem-cell activation [25]. This process is crucial to both normal embryonic development and cancer tumorigenesis, and thus is one of the best-studied in all of biology. The canonical Wnt pathway is a many-step process, summarized in Fig. 2a. First, an extracellular Wnt signal (such as the eponymous Wingless or Int-1 proteins, or one of their many analogues) interacts with two intermembrane proteins: Frizzled and LRP. Inside the cell, this complex binds to Axin,

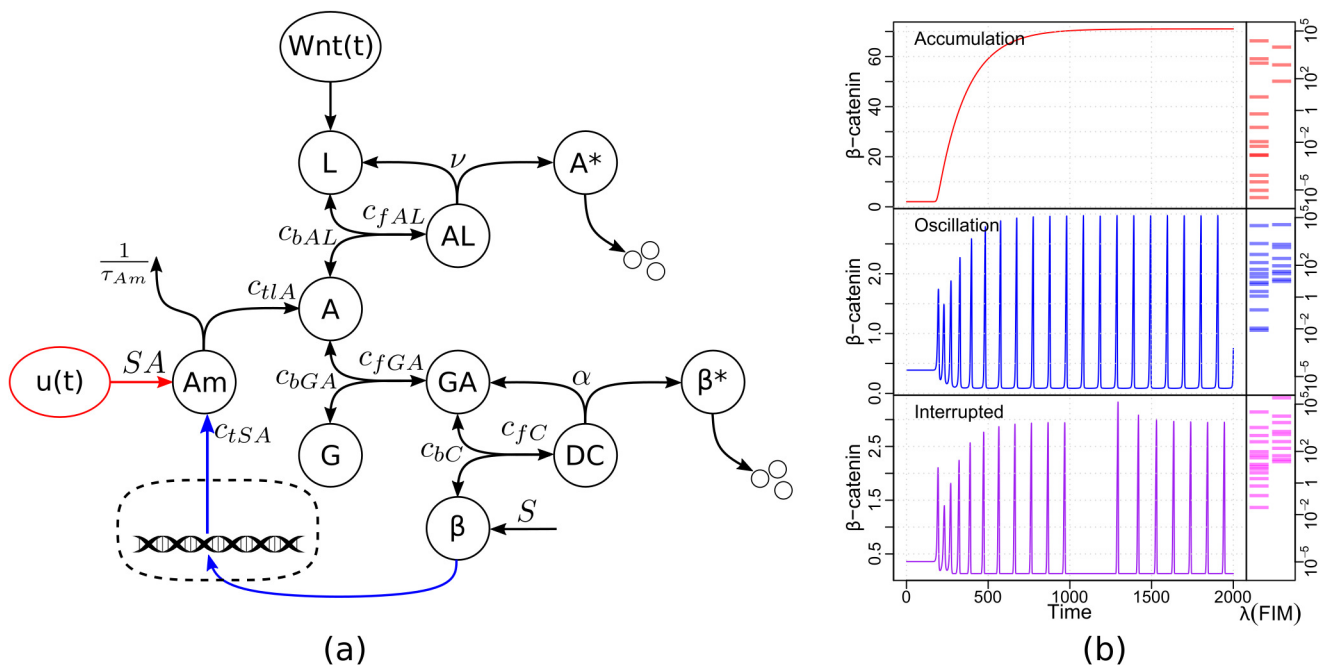


FIG. 2: (a) A network diagram showing the “full” model of the Wnt pathway. The red indicates mechanisms that are unique to the accumulation model, and blue indicates mechanisms unique to the oscillation model. (b) Three possible behaviors of beta-catenin in response to Wnt. The accumulation [18] and oscillation [19] behaviors are known to occur naturally, while behaviors similar to the interrupted behavior have been reported in [20–24].

thereby removing it from the APC-GSK3-Axin complex which normally degrades  $\beta$ -catenin.  $\beta$ -catenin is now free to accumulate and interact with DNA-associated proteins such as TCF to promote cell division [26, 27] This “accumulation phenomenon” is well-documented in the literature [18, 28] and illustrated in Fig. 2b.

A mass balance model of even this simple outline of the pathway contains over a dozen parameters, obscuring the relationship among output behaviors of  $\beta$ -catenin for different mechanisms. The problem is compounded by the fact that  $\beta$ -catenin is a transcription factor for many genes depending on the state of the cell. For example, during somitogenesis  $\beta$ -catenin activates Axin2 (a homolog of Axin) leading to a negative feedback loop, driving a limit cycle “oscillation phenomenon” that acts as a segmentation clock [19] (see Fig. 2b).

To model the relationship between these two phenomena, the relevant mechanisms at play in each, and how they might interact in new contexts, we construct a mechanistic model for each behavior. To model oscillation, we take that proposed by Jensen et al. [19]. We adapt this model to the accumulation phase by removing the negative feedback loop and replacing it with a controllable activation of Axin2, denoted by  $u(t)$  in Fig. 2. (One possible candidate for Axin2 activation is USP7 [29].) Fig. 2 presents a characteristic time series for each of these two models and generating equations in the supplement. In each case, the system begins in steady state, and a Wnt stimulus is introduced at 200 minutes. In

the first case,  $\beta$ -catenin accumulates and equilibrates at a new steady state [18, 28]. In the second case, the negative feedback loop triggers a Hopf bifurcation leading to sustained oscillations[19].

Each model has 14 parameters and a sloppy model analysis [30, 31] indicates many parameters are unidentifiable when fit to their respective time series. The right panels in Fig. 2b give the eigenvalues of the FIM for each model. We remove irrelevant parameters (small eigenvalues in the FIM) using the Manifold Boundary Approximation Method (MBAM) [15]. Fig. 3a summarizes the Hasse diagram of the MBAM-reduced models. The accumulation behavior is minimally described by three parameters while the oscillation phenomenon requires nine.

The MBAM reductions are not black boxes. Although the reduced models do abstract away many specific details, they retain vestiges of the full mechanisms, analogous to the SI and IR models in our epidemiology example. To relate these behaviors, we now seek the *supremum* of these two minimal representations. However, unlike the simple example, the minimal Wnt models contain partially overlapping combinations of parameters, so the construction is non-trivial.

Each reduction can be rewritten as a single parameter taken to zero. For example, consider an equilibrium approximation, i.e.,  $c_f, c_b \rightarrow \infty$ . This can be rewritten as a time constant going to zero  $\tau_f = 1/c_f \rightarrow 0$  and a nonzero equilibrium constant  $K_D = c_b/c_f$ . This form, however, is not unique as we could also have chosen  $\tau_b = 1/c_b \rightarrow 0$ .

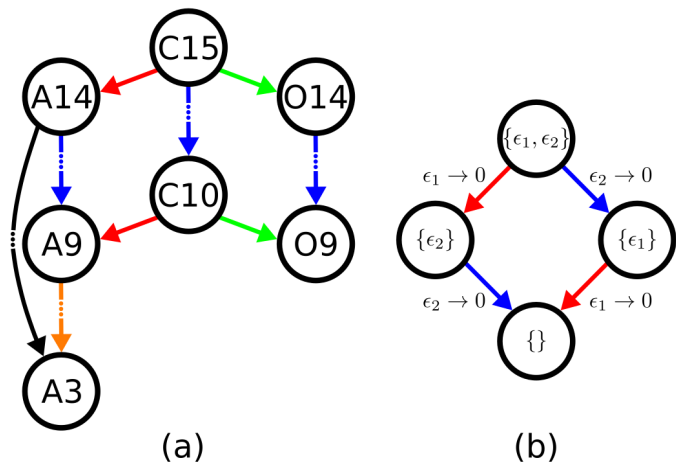


FIG. 3: (a) The Hasse diagram of key reduced models for the Wnt system. The nodes (models) are labeled by “A” for accumulation, “O” for oscillation, “C” for combined, as well as the number of parameters each model contains. The black line represents the original sequence of reduced accumulation models and the blue line represents the new sequence with parameter limits reordered to match those in the oscillation models. The central, blue arrow shows that the original model can be reduced to the supremal model using the same set of limits used to arrive at A9 and O9. Details about the model equations and sequence of limits can be found in the supplemental material. (b) A general example of the diamond property. Consider a model with  $N$  parameters containing two parameters  $\epsilon_1$  and  $\epsilon_2$ . The diamond property states that the order in which parameters can be removed commutes. The same model with  $N - 2$  parameters can be reached by first taking either  $\epsilon_1$  or  $\epsilon_2$  to zero, and then taking the other to zero. The diamond property is used to reorder the limits of a sequence, to build a supremal model.

For all equilibrium approximations we adopt the first as a standard form.

Next, we observe that the same reduced models can be derived by applying the same approximations in a different order. Commuting the order of reductions creates a diamond motif in the Hasse diagram, as illustrated in Fig. 3b. Because of the ambiguity in which parameters are used to label reductions, consecutive limits including the same parameters can obscure this commutation relation. For example, consider the consecutive limits of an equilibrium approximation ( $c_{bGA} \rightarrow \infty$ ,  $c_{fGA} \rightarrow \infty$  with  $c_{bGA}/c_{fGA}$  constant and finite) followed by an irreversible approximation ( $c_{bGA}/c_{fGA} \rightarrow 0$ ,  $c_{fAL} \rightarrow \infty$ ). Reparameterizing as  $\epsilon_1 = 1/c_{fGA}$ ,  $\epsilon_2 = 1/c_{fAL}$ , and  $\phi = c_{fAL}c_{bGA}/c_{fGA}$  makes the diamond property apparent. The two limits of the diamond property can now be written as  $\epsilon_1 \rightarrow 0$  and  $\epsilon_2 \rightarrow 0$ . Writing all of the reductions in a standard form allows us to identify the common approximations to each chain of reduced mod-

els.

We now describe our algorithm for constructing a supremal model, and illustrate with Wnt. 1) We identify the approximations common to both reductions. 2) We recursively use the diamond property to reorder the limits applied to the accumulation and oscillation models, putting those limits that overlap at the top, relabeling as necessary at each step. This is done by putting all different types of limits, e.g. equilibrium approximations, in a standard form. 3) We next apply only those approximations that are shared by both reductions, resulting in two nine-parameter models. 4) We take the union of the terms in these models, just as we did for the SIR example, to construct the supremum.

To illustrate step 4, consider the dynamic equation for a renormalized Axin2 mRNA,  $y = c_{tIA} [Am]$ . The dynamics for the 9-parameter accumulation and oscillation models respectively are

$$\frac{dy}{dt} = -\frac{1}{\tau_{Am}}y + \theta_1 u(t) \quad (2)$$

$$\frac{dy}{dt} = -\frac{1}{\tau_{Am}}y + \theta_2 [\beta]^2. \quad (3)$$

Taking the union of terms in these equations gives the dynamic equation for the supremal model

$$\frac{dy}{dt} = -\frac{1}{\tau_{Am}}y + \theta_1 u(t) + \theta_2 [\beta]^2. \quad (4)$$

A second algorithm for finding the supremum of the reduced models is to apply the common approximations (step one above) to the head node of the Hasse diagram, illustrated by the blue line connecting C15 to C10 in Fig. 3. While the first method constructs the union of the relevant mechanisms in both minimal models, the second method constructs the intersection of the approximations from both reductions. These two algorithms reflect a general duality inherent to POSets.

By including both the feedback loop and external control, the supremum enables the accumulation and oscillation phenomena, as well as additional behaviors neither A14 nor O14 can produce. Fig. 2b demonstrates one such example, the “interrupted” behavior, in which the external control modulates the phase of the oscillation. Regular oscillatory behavior in the Wnt pathway is well-known *in vivo* from the segmentation clock in vertebrate embryos along the anterior-posterior axis to establish, for example, the repeating pattern of vertebrae and ribs [32]. These regular oscillations can have their period and phase modified, stopped, or restarted through manipulation of “dorsalizing” or “ventralizing” molecular regulators, much like the interrupted behavior we see in the supremal model [20–24]. To validate our model, we apply MBAM to the head node using the predictions for this novel behavior. The result of this reduction is the same supremal model constructed by the two algorithms, indicating that the supremum is the simple model that would have been selected had observations been available for this behavior.

Classical psychological theories use geometric constructions to represent analogical relationships. Most notably, in the parallelogram model [33], an analogy such as man:woman::king:queen is represented as four corners of a parallelogram with analogical relationships forming parallel sides [34]. Such constructions are widespread in AI applications ranging from recommender systems [35] to natural language processing [36]. The key property, however, is the topological relationship between analogous elements [37] that for parallelograms form the same diamond motif as in Fig. 3. Thus, our supremum construction identifies the mathematical “analogies” between models by teasing out the common mechanisms or analogous reductions (see the colored arrows in Fig. 3). The approximations in linking model C15 to model C10 are the same as those connecting model A14 to model A9, i.e., C15:C10::A14:A9. The colored arrows indicate the many other possible analogies that could be drawn among the models.

The supremum principle shows promise for transferring predictability to truly new domains. For example, the SI and IR models fail in the intermediate regime, and the accumulation and oscillation models fail in the interrupted regime, but the supremal models in each case are able to embrace all three behaviors. This is more than the simple generalization of, e.g., multi-task learning (MTL) [38]. Supremal models apply in a more global way; they

aim to improve the transferability of a model to new data from a completely new regime.

Beyond the appeal of elegant, simplified models, we expect supremal models to be of broad practical use; for example, in systems that need a controller to move between two behavioral states, but cannot be fully modelled due to a lack of information, or excessive complexity, or both. Such systems include shifting from diseased to healthy states in medical contexts, failing to stable power grids in electrical engineering, ductile to brittle structures in material science, and collapsed to restored resources in ecosystem-based management. Supremal models are also designed for maximal simplicity while retaining some transferability, i.e., attempting to predict in regimes not yet examined, such as in climate modeling, prosperous non-growth-based economics, and human behavior during a pandemic. Practitioners from a wide variety of fields will find supremum modeling a powerful addition to their toolboxes.

This work was supported by the US National Science Foundation under Award NSF-1753357 (CP, CA, MKT), CMMT-1834332 (CP, MKT), and EPCN-1710727 (CA, MKT). We thank Sean Warnick, Kolten Barfuss, and Alex Stankovic for helpful conversations. We thank Ben Francis, Dan Karls, Ellad Tadmor, and Ryan Elliott for comments on the manuscript.

- 
- [1] J. Baxter, *Journal of Artificial Intelligence Research* **12**, 149 (2000).
- [2] K. Weiss, T. M. Khoshgoftaar, and D. Wang, *Journal of Big Data* **3**, 9 (2016).
- [3] K. S. Brown and J. P. Sethna, *Physical Review E* **68**, 021904 (2003).
- [4] K. S. Brown, C. C. Hill, G. A. Calero, C. R. Myers, K. H. Lee, J. P. Sethna, and R. A. Cerione, *Physical Biology* **1**, 184 (2004).
- [5] J. J. Waterfall, F. P. Casey, R. N. Gutenkunst, K. S. Brown, C. R. Myers, P. W. Brouwer, V. Elser, and J. P. Sethna, *Physical Review Letters* **97**, 150601 (2006).
- [6] B. B. Machta, R. Chachra, M. K. Transtrum, and J. P. Sethna, *Science* **342**, 604 (2013).
- [7] S.-i. Amari and H. Nagaoka, *Methods of information geometry*, Vol. 191 (American Mathematical Soc., 2007).
- [8] M. K. Transtrum, B. B. Machta, and J. P. Sethna, *Phys. Rev. Lett.* **104**, 060201 (2010).
- [9] C. H. LaMont and P. A. Wiggins, *Physical Review E* **99**, 052140 (2019).
- [10] K. N. Quinn, H. Wilber, A. Townsend, and J. P. Sethna, *Physical Review Letters* **122**, 158302 (2019).
- [11] M. K. Transtrum, B. B. Machta, and J. P. Sethna, *Physical Review E* **83**, 036701 (2011).
- [12] B. M. Lake, T. D. Ullman, J. B. Tenenbaum, and S. J. Gershman, *Behavioral and Brain Sciences* **40**, e253 (2017).
- [13] T. Webb, Z. Dulberg, S. Frankland, A. Petrov, R. O’Reilly, and J. Cohen, in *Proceedings of the 37th International Conference on Machine Learning*, Proceedings of Machine Learning Research, Vol. 119, edited by H. D. III and A. Singh (PMLR, 2020) pp. 10136–10146.
- [14] A. F. Brouwer and M. C. Eisenberg, arXiv:1802.05641 [math] (2018), arXiv: 1802.05641.
- [15] M. K. Transtrum and P. Qiu, *Physical Review Letters* **113**, 098701 (2014).
- [16] Although this approximation is constructed by taking  $\gamma \rightarrow 0$ , it does not require the “true” value of  $\gamma$  to be small. Rather, the role of the recovery mechanism can be compressed into a simpler model with an effective infection rate, similar to the effective electron mass in a condensed matter system.
- [17] M. K. Transtrum, G. Hart, and P. Qiu, *CoRR* (2014), arXiv:1409.6203 [physics.data-an].
- [18] L. Goentoro and M. W. Kirschner, *Molecular Cell* **36**, 872 (2009).
- [19] P. B. Jensen, L. Pedersen, S. Krishna, and M. H. Jensen, *Biophysical Journal* **98**, 943 (2010).
- [20] I. H. Riedel-Kruse, C. Müller, and A. C. Oates, *Science* **317**, 1911 (2007).
- [21] S. Gibb, A. Zagorska, K. Melton, G. Tenin, I. Vacca, P. Trainor, M. Maroto, and J. K. Dale, *Developmental Biology* **330**, 21 (2009).
- [22] A. Goldbeter and O. Pourquié, *Journal of Theoretical Biology* **252**, 574 (2008).
- [23] C. Gomez, E. M. Özbudak, J. Wunderlich, D. Baumann, J. Lewis, and O. Pourquié, *Nature* **454**, 335 (2008).
- [24] Y. Rui, Z. Xu, B. Xiong, Y. Cao, S. Lin, M. Zhang, S. C. Chan, W. Luo, Y. Han, Z. Lu, Z. Ye, H. M. Zhou, J. Han, A. Meng, and S. C. Lin, *Developmental Cell* **13**,

- 268 (2007).
- [25] R. Nusse and H. Clevers, *Cell* **169**, 985 (2017).
- [26] C. Y. Logan and R. Nusse, *Annual Review of Cell and Developmental Biology* **20**, 781 (2004).
- [27] Y. Ding, S. Su, W. Tang, X. Zhang, S. Chen, G. Zhu, J. Liang, W. Wei, Y. Guo, L. Liu, Y.-G. Chen, and W. Wu, *Journal of Cell Science* **127**, 4833 (2014).
- [28] E. Lee, A. Salic, R. Krüger, R. Heinrich, and M. W. Kirschner, *PLOS Biology* **1**, e10 (2003).
- [29] L. Ji, B. Lu, R. Zamponi, O. Charlat, R. Aversa, Z. Yang, F. Sigoillot, X. Zhu, T. Hu, J. S. Reece-Hoyes, C. Russ, G. Michaud, J. S. Tchorz, X. Jiang, and F. Cong, *Nature Communications* **10**, 4184 (2019).
- [30] R. N. Gutenkunst, J. J. Waterfall, F. P. Casey, K. S. Brown, C. R. Myers, and J. P. Sethna, *PLOS Computational Biology* **3**, e189 (2007).
- [31] M. K. Transtrum, B. B. Machta, and J. P. Sethna, *Physical Review E* **83**, 036701 (2011).
- [32] O. Pourquie, *Science* **301**, 328 (2003).
- [33] D. E. Rumelhart and A. A. Abrahamson, *Cognitive Psychology* **5**, 1 (1973).
- [34] J. C. Peterson, D. Chen, and T. L. Griffiths, *Cognition* **205**, 104440 (2020).
- [35] C. Musto, in *Proceedings of the fourth ACM conference on Recommender systems* (2010) pp. 361–364.
- [36] J. N. Reid and A. N. Katz, *Metaphor and Symbol* **33**, 280 (2018).
- [37] D. Gentner, *Cognitive Science* **7**, 155 (1983).
- [38] R. Caruana, *Machine Learning* **28**, 41 (1997).